Serendipitous discovery of a dying Giant Radio Galaxy associated with NGC 1534, using the Murchison Widefield Array

Natasha Hurley-Walker[A], Melanie Johnston-Hollitt[B], Ron Ekers[C,A], Richard Hunstead[D],
Elaine M. Sadler[D], Luke Hindson[B], Paul Hancock[A,E], Gianni Bernardi[F,G,H],
Judd D. Bowman[I], Frank Briggs[E,J], Roger Cappallo[K], Brian Corey[K],
Avinash A. Deshpande[L], David Emrich[A], Bryan M. Gaensler[E,D], Robert Goeke[K],
Lincoln Greenhill[H], Bryna J. Hazelton[M], Jacqueline Hewitt[N], David L. Kaplan[O],
Justin Kasper[H], Eric Kratzenberg[K], Colin Lonsdale[K], Mervyn Lynch[A],
Daniel Mitchell[C,E], Russell McWhirter[K], Miguel Morales[M], Edward Morgan[N],
Divya Oberoi[P], André Offringa[E,J], Stephen Ord[A,E], Thiagaraj Prabu[L], Alan Rogers[K],
Anish Roshi[Q], Udaya Shankar[L], K. Srivani[L], Ravi Subrahmanyan[L,E],
Steven Tingay[A,E], Mark Waterson[A,J], Randall B. Wayth[A,E], Rachel Webster[E,R],
Alan Whitney[K], Andrew Williams[A], Chris Williams[N]

Email: nhw@icrar.org
[A] *International Centre for Radio Astronomy Research, Curtin University, Bentley, WA 6102, Australia*
[B] *School of Chemical & Physical Sciences, Victoria University of Wellington, Wellington 6140, New Zealand*
[C] *CSIRO Astronomy and Space Science, Marsfield, NSW 2122, Australia*
[D] *Sydney Institute for Astronomy, School of Physics, The University of Sydney, NSW 2006, Australia*
[E] *ARC Centre of Excellence for All-sky Astrophysics (CAASTRO)*
[F] *Square Kilometre Array South Africa (SKA SA),3rd Floor, The Park, Park Road, Pinelands, 7405, South Africa*
[G] *Department of Physics and Electronics, Rhodes University, PO Box 94, Grahamstown, 6140, South Africa*
[H] *Harvard-Smithsonian Center for Astrophysics, 60 Garden Street, Cambridge, MA, 02138, USA*
[I] *School of Earth and Space Exploration, Arizona State University, Tempe, AZ 85287, USA*
[J] *Research School of Astronomy and Astrophysics, Australian National University, Canberra, ACT 2611, Australia*
[K] *MIT Haystack Observatory, Westford, MA 01886, USA*
[L] *Raman Research Institute, Bangalore 560080, India*
[M] *Department of Physics, University of Washington, Seattle, WA 98195, USA*
[N] *Kavli Institute for Astrophysics and Space Research, Massachusetts Institute of Technology, Cambridge, MA 02139, USA*
[O] *Department of Physics, University of Wisconsin–Milwaukee, Milwaukee, WI 53201, USA*
[P] *National Centre for Radio Astrophysics, Tata Institute for Fundamental Research, Pune 411007, India*
[Q] *National Radio Astronomy Observatory, Charlottesville and Greenbank, USA*
[R] *School of Physics, The University of Melbourne, Parkville, VIC 3010, Australia*

arXiv:1412.3856v1 [astro-ph.GA] 11 Dec 2014

ABSTRACT

Recent observations with the Murchison Widefield Array at 185 MHz have serendipitously unveiled a heretofore unknown giant and relatively nearby ($z = 0.0178$) radio galaxy associated with NGC 1534. The diffuse emission presented here is the first indication that NGC 1534 is one of a rare class of objects (along with NGC 5128 and NGC 612) in which a galaxy with a prominent dust lane hosts radio emission on scales of $\sim 700 \, \mathrm{kpc}$. We present details of the radio emission along with a detailed comparison with other radio galaxies with disks. NGC 1534 is the lowest surface brightness radio galaxy known with an estimated scaled 1.4-GHz surface brightness of just $0.2 \, \mathrm{mJy \, arcmin}^{-2}$. The radio lobes have one of the steepest spectral indices yet observed: $\alpha = -2.1 \pm 0.1$, and the core to lobe luminosity ratio is $< 0.1\%$. We estimate the space density of this low brightness (dying) phase of radio galaxy evolution as $7 \times 10^{-7} \, \mathrm{Mpc}^{-3}$ and argue that normal AGN cannot spend more than 6% of their

1 INTRODUCTION

Giant Radio Galaxies (GRG) are characterised by larger linear size (usually $\geqslant 700\,\mathrm{kpc}$; see e.g. Saripalli et al. 2005), and a radio spectrum that is much steeper than normal radio galaxies. These galaxies have a low surface brightness and without an active nucleus to provide fresh particle injection, they probably represent a short-lived, final stage of radio galaxy evolution (e.g. Murgia et al. 2011). The short timescale of this final phase of evolution makes these sources rare. The typically low surface brightness of GRGs means that only surveys with high brightness sensitivity are able to detect them.

Detection of GRGs at low ($\leqslant 300\,\mathrm{MHz}$) radio frequencies reveals details of the low-energy electron population present in the radio lobes which in turn provides information on the acceleration processes required to generate and maintain the emission. Instruments such as the Low Frequency Array (LOFAR; van Haarlem et al. 2013), the Giant Metrewave Radio Telescope (GMRT) and the Murchison Widefield Array (MWA; Lonsdale et al. 2009; Tingay et al. 2013) are thus important in the study of this class of object and have the potential to detect such sources in greater numbers. In particular, LOFAR and MWA are expected to detect older "dying" GRGs whose radio lobes are comprised of old plasmas of low-energy electrons, whose steep spectra make them invisible at high radio frequencies. Here we present the serendipitous detection of one such previously-unknown GRG associated with the lenticular galaxy NGC 1534.

The Murchison Widefield Array is a new low-frequency telescope operating at the Murchison Radio-astronomy Observatory in remote Western Australia. Operating between 80 and 300 MHz, the MWA represents the first fully operational precursor instrument for the Square Kilometre Array (SKA).

During Director's Discretionary Time (DDT) observations made in late August 2013, the bright radio source PKS 0408 − 65 was observed at 185 MHz as a phase calibrator. The full-width-half-maximum of the primary beam of the MWA is $\approx 30°$ so the $\approx 900\,\mathrm{deg}^2$ surrounding this source were also imaged during the routine calibration process. An unusual source of low surface-brightness extended emission was serendipitously detected, and further images were made from the available observations in order to determine its nature.

This paper is laid out as follows. Section 2 describes the observations, the calibration and imaging strategy used in data reduction, and the flux density calibration procedures, including correcting for the MWA primary beam. Section 3 describes the properties of the radio source using MWA and archival data. Section 4 discusses the impact of the detection of this source, and Section 5 concludes the paper with future observing prospects for radio galaxies of a similar nature.

We adopt a standard set of cosmological parameters throughout with $H_0 = 73\,\mathrm{km\,s^{-1}Mpc^{-1}}$, $\Omega_m = 0.27$ & $\Omega_\Lambda = 0.73$. At $z = 0.017802 \pm 0.000017$ (Paturel et al. 2002), the luminosity distance of NCG 1534 is 74.2 Mpc, and 1 arcmin corresponds to 20.8 kpc.

All position angles are measured from North through East (i.e. counter-clockwise). All equatorial co-ordinates are J2000. Figures use the "cubehelix" colour scheme (Green 2011).

2 OBSERVATIONS AND DATA REDUCTION

As detailed by Tingay et al. (2013), the MWA consists of 128 32-dipole antenna "tiles" distributed over an area approximately 3 km in diameter. Each tile observes two instrumental polarisations, "X" (16 dipoles oriented East-West) and "Y" (16 dipoles oriented North-South). The signals from the tiles are collected by 16 in-field receiver units, each of which services eight tiles.

During the observations made on 2013 Aug 31, 126 of the 128 tiles were functioning normally. As the potential GRG was not the primary focus of the observations, only 5.5 minutes of data were recorded, in three separate 1.8-minute observations at UTC 19:37:28, 20:01:28 and 20:25:27. Data were collected at 0.5-second, 40-kHz resolution in a 30.72-MHz band centred at 184.9 MHz (hereafter written as 185 MHz). The compact antenna layout of the MWA gives it extremely high surface brightness sensitivity: $\sigma_T \approx 20\,\mathrm{mK}$ ($6\,\mathrm{mJy\,arcmin^{-2}}$) for these 5-minute observations. The large number of elements results in very good u, v-coverage, and thus a well-behaved synthesised beam and excellent image quality, even for such a short observing time.

As the observations were originally made for the purpose of calibration, they are easily calibrated by using a model of PKS 0408 − 65 and running `bandpass`, an algorithm from the Common Astronomy Software Applications (CASA[1]), to produce per-observation, per-antenna, per-polarisation, per-channel gains, which were then applied. The data are imaged using a standard `clean`, with a pixel resolution of $0\rlap{.}{'}75$, an image size of 4000×4000 pixels, and a threshold of $3\sigma \approx 0.3\,\mathrm{Jy\,beam^{-1}}$ (measured after an initial shallow clean). We phase to PKS 0408 − 65, and ignore wide-field effects, which are not significant at the distance NGC 1534 lies from this phase centre ($\approx 3°$). Most importantly, we use a "robust" or "Briggs" (Briggs 1995) weighting scheme, with a robustness parameter of $+1.0$, which offers a compromise between sensitivity to large-scale structure (a four-fold improvement in brightness sensitivity compared to uniform weighting) and a synthesised beam with reasonably well-suppressed sidelobes ($\lesssim 10\%$ compared to $\lesssim 15\%$ for a naturally-weighted beam and $\lesssim 5\%$ for a uniformly-weighted beam).

Following Hurley-Walker et al. (2014), we use a mosaicking strategy to combine our observations into a single image. As each observation is self-calibrated, and the ionospheric conditions were calm (i.e. no significant direction-dependent position distortions) there is no ionospheric blurring when the images are combined. The point spread function is the average of the synthesised beams of the three individual observations: $305'' \times 231''$, at a position angle of $139\rlap{.}{°}1$.

Each snapshot was taken with a different delay setting on the MWA analogue beamformers; an analytic primary beam model was calculated for each setting and used to weight and correct the images during the mosaicking step. This results in a smoothly-varying flux scale across the map, as the primary beam model is not yet reliable at 185 MHz, 40° from zenith, but has no sharp or discontinuous features.

Following the method of Hindson et al. (2014) we account for this flux calibration error and determine a flux

---

[1] http://casa.nrao.edu/

scale relative to known, strong sources. We select a sample of 14 suitable flux calibrators drawn from the Parkes compilation of radio sources (Wright & Otrupcek 1990) (which is itself a compilation from several surveys, most notably Large et al. (1981)). These sources were selected with the following criteria: be unresolved in all MWA bands, have a flux density greater than 1 Jy at 843 MHz and be well-fitted by a simple power-law with no sign of curvature at low frequencies. For these sources, we fit the spectral profile between 408 and 5000 MHz using the power-law relation $S \propto \nu^{\alpha}$. We then extrapolate this fitted power-law to 185 MHz and scale the flux in our MWA map at the position of each flux calibrator accordingly. To account for the variation of the flux density scale across the image we perform cubic interpolation using the scale factors of our 14 flux calibrators to determine a position-dependent flux density scale in the region covered by the 14 flux calibrators ($\approx 20 \deg^2$ around NGC 1534). We verify the accuracy of the applied flux density scale by comparing the flux density estimates in our scaled 185 MHz map to the predicted flux density at 185 MHz for five test sources: PKS 0400-613, PKS 0430-624, PKS 0405-640, PMN J0340-6507 and PMN J0406-6050. We present the predicted and corrected flux densities for these sources in Table 1. Since the test flux densities themselves are extrapolations, and the observed error does not increase with angular distance from NGC 1534, we expect the dominant source of error to be the assumption that both the flux calibration and test sources have power-law spectra below 400 MHz. In this region of the sky there is currently no better option; we estimate the contribution of the residual flux scaling error to our flux density estimates to be $\sim 10\%$.

3   RESULTS

Figure 1 presents the robust $+1.0$ weighted MWA image of 10% of the field, showing that the data have reasonably consistent noise characteristics. The Large Magellanic Cloud is to the lower-left and diffuse Galactic emission is evident in the upper right and lower middle of the image. In the centre of the field we clearly see two diffuse patches of low-surface-brightness emission significantly above the Galactic emission in the image. The morphology is reminiscent of a double-lobed radio galaxy, but with wide lobes, and no obvious hot spots or core. The inset shows a zoom of the central source and two sources to the south; the eastern structure is revealed in higher-resolution radio data (e.g. the Sydney University Molonglo Sky Survey (SUMSS; Bock, Large & Sadler 1999; Mauch et al. 2003) at 843 MHz) as two compact radio sources confused together by the large MWA synthesised beam, and the western structure is an FR-II radio galaxy aligned N-S.

It is not entirely straightforward to measure the noise properties of the map, given that it contains a large amount of diffuse structure on different scales. We employ the technique of Hancock et al. (in prep), in which background and noise images are determined using a spatial filter similar to a box-car filter. This is an efficient implementation ideal for large radio images compared to standard algorithms optimised for small optical images. The background image is calculated as the median of pixels within a rectangular region of size 20×20 synthesised beams ($\approx 2 \deg^2$). The noise

image is calculated from the inter-quartile range of the median subtracted pixels over the same region. Since radio images have a high spatial correlation, we calculate the median and inter-quartile range on a grid with a spacing of 4×4 pixels, and linearly interpolate to form a final image. We measure the background level as $5 \, \mathrm{mJy \, beam^{-1}}$, and subtract it from our measured flux densities; the RMS is calculated as $100 \, \mathrm{mJy \, beam^{-1}}$ in the vicinity of NGC 1534. (This agrees well with the more manual method of measuring the mean and RMS in nearby regions that have no obvious source peaks.)

We use the RMS measurement of $100 \, \mathrm{mJy \, beam^{-1}}$ as an estimate of the noise in the image, and measure the flux density of the radio galaxy lobes by integrating down to multiples of 2 and 3 times this value. First, we measure the total flux density of the source by integrating down to $2 \, \sigma$. We then measure the relative power of the northern and southern lobes by integrating each lobe down only to $3 \, \sigma$. We multiply this ratio by the 2-σ integrated flux density to obtain the flux densities of the two lobes. We estimate the total 185 MHz flux density of the radio lobes to be 4.8 ± 0.5 Jy and the flux densities to be 3.0 ± 0.3 and 1.8 ± 0.2 Jy for the southern and northern lobes, respectively (Table 2).

Measured from the 2-σ contours to the NW and SE, the angular extent of the lobes is 33 arcmin, or 700 kpc in our cosmology. They lie at an angle of $334°$ from North through East.

3.1   Host galaxy

Figure 2 shows the MWA radio contours overlaid on the Digitized Sky Survey (DSS) red field. At the centre of these two diffuse patches we see a relatively bright 13.7 mag galaxy at a redshift of 0.0178, NGC 1534: see Table 3. The galaxy has an obvious disk component with a dust lane as well as a dominant nuclear bulge. de Vaucouleurs et al. (1991) classify it as SA0/a?(rs) edge-on: a lenticular, with the possibility of being a spiral. Spiral structure is somewhat visible in the optical image. Crook et al. (2007) associate NGC 1534 with the galaxy groups LDC 292 and HDC 269, which have 17 and 3 members, respectively.

The position angle of the lobes is well-aligned with the minor axis of the host galaxy dust lane (Table 3), with a difference of only $6°$; this is consistent with other GRGs which exhibit such minor axis alignment (Saripalli & Subrahmanyan 2009) and supports NGC 1534 as the host galaxy. We note that there is no radio source coincident with NGC 1534 itself, at any frequency.

3.2   Other radio images

The Sydney University Molonglo Sky Survey (SUMSS; Bock, Large & Sadler 1999; Mauch et al. 2003) at 843 MHz is the highest-resolution low-frequency radio catalogue covering this region. The SUMSS image shows four contaminating point sources within the envelope of the diffuse radio emission, whose positions and fluxes are given in Table 4, and whose positions are indicated by "+"s in the left panel of Figure 3. The contaminating point sources are unresolved by all other instruments discussed in this paper. An average spectral index, $\alpha = -0.7$ was used to estimate the flux densities at other frequencies, and these were subtracted from

Table 1. Test sources to examine the accuracy of the flux re-scaling procedure described in Section 2.

Source Name	Flux Density Predicted (Jy)	Corrected (Jy)	Residual difference (mJy)	Angular distance from NGC 1534 (deg.)
PKS 0405-640	3.06	2.88	$+18 \pm 6$	0.93
PKS 0400-613	1.66	1.35	$+31 \pm 19$	0.96
PMN J0406-6050	1.86	1.50	$+36 \pm 12$	2.06
PKS 0430-624	3.64	3.76	-12 ± 3	2.75
PMN J0340-6507	3.76	4.42	-66 ± 50	4.86
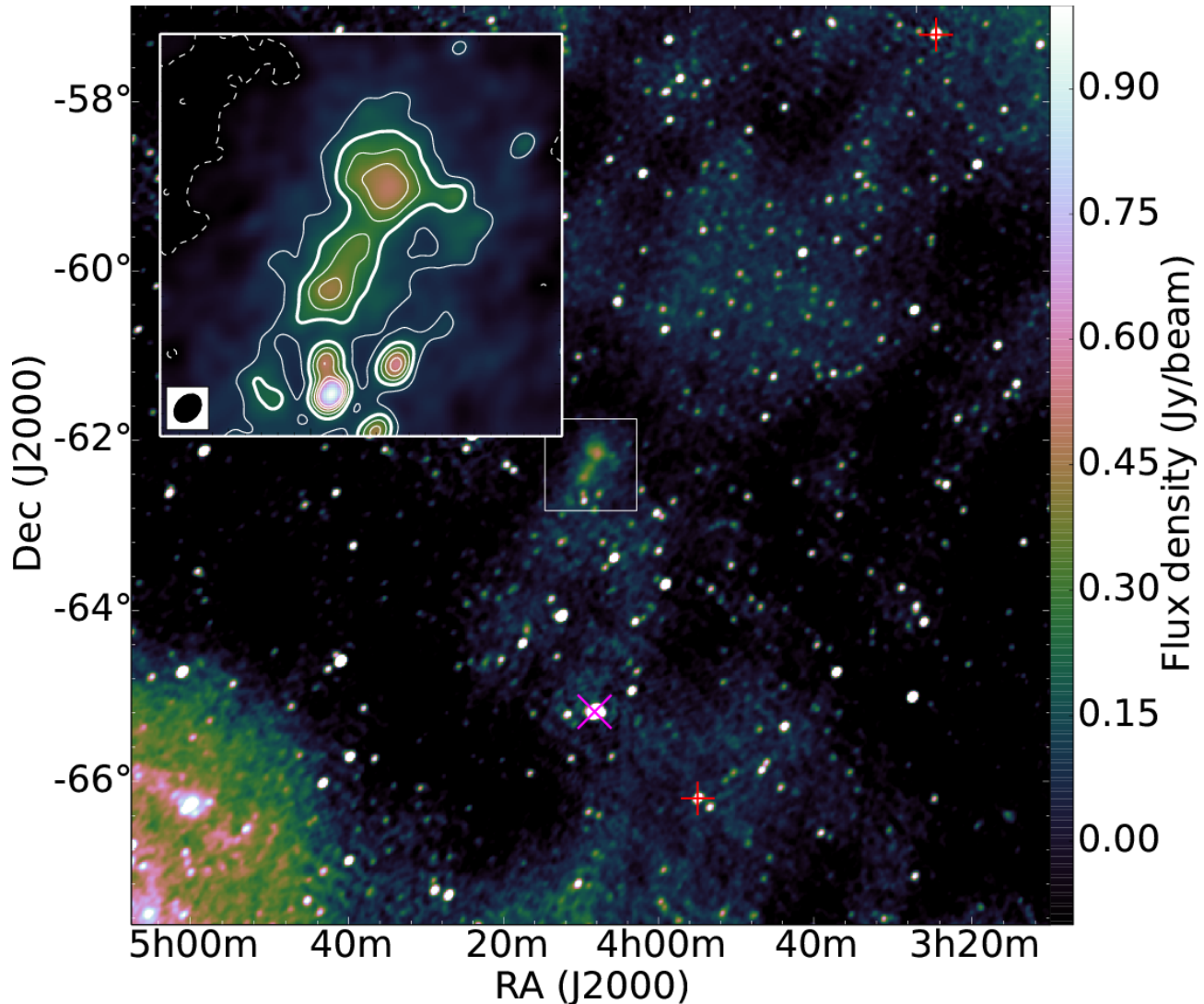
Figure 1. 185 MHz image of NCG 1534, showing the surrounding $100\,\mathrm{deg}^2$ with a linear colourscale between -0.1 and $1.0\,\mathrm{Jy\,beam}^{-1}$. The two sources marked with red "+"s are two of the flux calibration sources described in Section 2. The phase calibrator, PKS 0408 − 65 is marked with a magenta "X". The inset image shows a zoomed view of the radio lobes, with solid contours starting at $0.1\,\mathrm{Jy\,beam}^{-1}$ and increasing in $\sigma = 100\,\mathrm{mJy\,beam}^{-1}$ increments to $+0.6\,\mathrm{Jy\,beam}^{-1}$, a thicker contour at 2σ, and a dashed contour at -1σ. The PSF is shown as a solid ellipse, of dimensions $305'' \times 231''$, at a position angle of $139°.1$. Henceforth, all images are shown with the same size and sky location as this inset image.

Table 2. Integrated flux densities for the MWA, MRCR, SUMSS and CHIPASS data, after subtraction of contaminating point sources and masking of negative pixels. Errors on the MWA flux densities may be taken as 10 %, due to the dominant calibration error from the flux calibration process described in Section 2. The SUMSS error bars are calculated as the RMS of the local region in the smoothed map. The MRCR data point with a "*" is a simple doubling of the upper limit given the morphology shown in Figure 4.

Instrument	Frequency / MHz	Flux density / mJy		
		NW	SE	Total
MWA	185	3000 ± 300	1800 ± 180	4800 ± 480
MRCR	408	> 260	> 150	$> 410, \sim 820*$
SUMSS	843	130 ± 20	80 ± 20	210 ± 20
CHIPASS	1400	< 45	< 27	< 72

Table 3. Properties of the host galaxy NGC 1534.

Property	Value	Reference
Position (J2000)	$04^h08^m46.066^s$ $-62°47'51''21$	Skrutskie et al. (2006)
Redshift	0.017802 ± 0.000017	Paturel et al. (2002)
Morphological type	SA0/a?(rs)	de Vaucouleurs et al. (1991)
IRAS 60μm flux density	0.332 ± 0.033 Jy	Neugebauer et al. (1984)
IRAS 100μm flux density	1.885 ± 0.188 Jy	Neugebauer et al. (1984)
Position angle of dust lane (N through E)	$250°$	Skrutskie et al. (2006)
H I mass	$< 1.0 \times 10^{10}$ M$_\odot$	Barnes et al. (2001)
M_K	-25.0	Skrutskie et al. (2006)
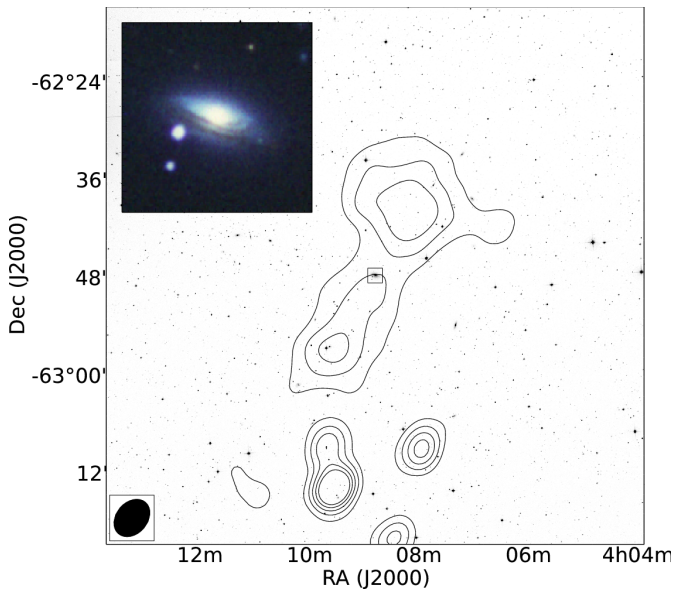
Figure 2. MWA 185-MHz contours starting at 2σ and proceeding in $\sigma = 100$ mJy increments, overlaid on the Digitized Sky Survey (DSS) Red image. NGC 1534 can be seen at the top of the southern lobe. The inset shows a false color image of NGC 1534, marked on the main image with a square; red represents the UK Schmidt infra-red image, green the the European Southern Observatory Red image, and blue the UK Schmidt Blue image. A dust lane is clearly visible.

any flux density measurement of the lobes which overlapped with their positions.

To highlight the small amount of structure on scales > 0°.5 detected by SUMSS, we convolve the image to match the MWA synthesised beam. The right panel of Figure 3 shows the resulting image with MWA 185-MHz contours overlaid:

the radio galaxy lobes are just visible. We calculate the integrated flux density as 209 mJy by summing the flux under the integration contours derived from the MWA data, and subtracting the contaminating sources as described above. The RMS noise on the smoothed SUMSS image is ≈ 20 mJy in this area so we ascribe a 10% error to this flux density measurement.

The Molonglo Reference Catalogue (MRC; Large et al. 1981) at 408 MHz also covers this region but only reaches a completeness flux density of 0.95 Jy. However, the survey itself goes far deeper, with an RMS noise level of $\sim$30–50 mJy, and a revised version known as MRCR (described in Broderick et al. 2007) has been created in image form (D.F. Crawford, private communication). The MRCR image in the vicinity of MWA J0408$-$6247 is unfortunately contaminated by the north-south sidelobes of PKS 0408$-$65 ($S_{408\,\mathrm{MHz}} = 51$ Jy), which is $3°$ due south, and attempts at deconvolution have left a negative residue. To place a lower limit of 410 mJy, on the flux density detected in the image, we masked all pixels of negative values, integrated under the same MWA contours, and subtracted the estimated contaminating source flux densities. As the side lobe cuts the source in half we can assume to first order that the total flux density is approximately 820 mJy.

We note that the shortest baseline of the Molonglo Cross is 15 m, so the MRCR should be sensitive to scales up to 2°.8, and SUMSS to scales up to 1°.4, which is sufficient to measure the flux density of the radio galaxy lobes, given the necessary sensitivity and the absence of image processing artefacts.

By reprocessing archival data from the HI Parkes All-Sky Survey (HIPASS), Calabretta, Staveley-Smith & Barnes (2014) present a 1.4 GHz continuum map of the sky south of Declination $+25°$ (CHIPASS). At the location of the radio lobes, the continuum 1.4 GHz (CHIPASS) image shows no obvious maximum, and the peak brightness temperature is
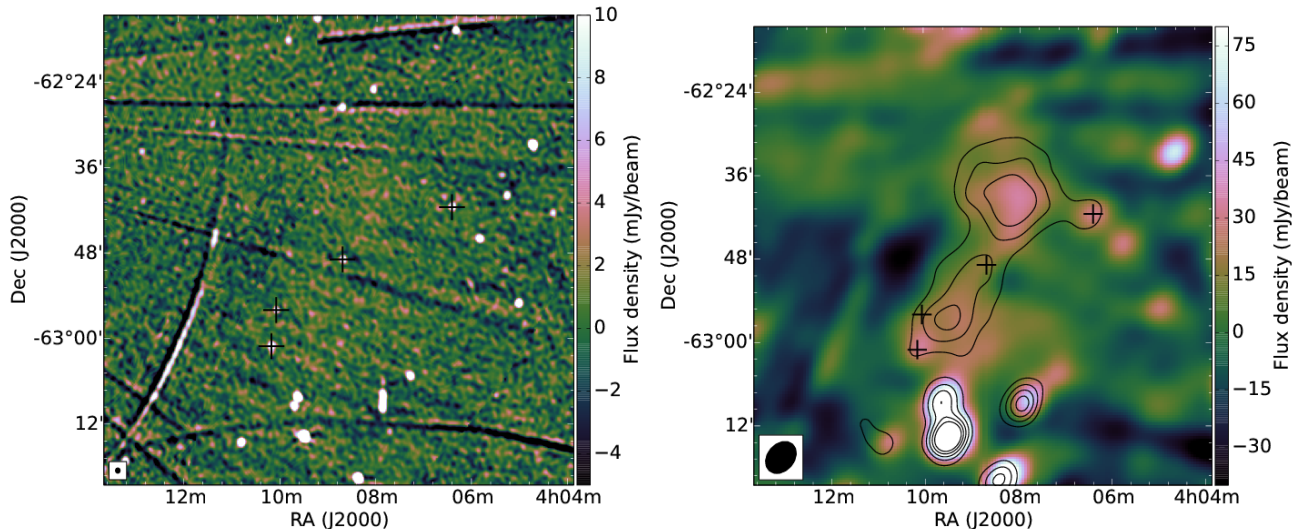
Figure 3. SUMSS 843 MHz image of the NCG 1534 region with the four SUMSS catalogue sources indicated with black crosses. The flux densities of these sources are given in Table 4. The left panel shows the original SUMSS image, and the right panel shows the image after convolution to match the MWA resolution. The arc-like artifacts in the SUMSS image are grating responses from the bright sources PKS 0408−65 and PKS 0420−62, and the linear features are radial artifacts from PKS 0420−62. The synthesised beams of SUMSS ($48'' \times 43''$; position angle 0°) and the MWA ($305'' \times 231''$; position angle 139°.1) are shown as filled ellipses in the lower-left corner of the left and right panels, respectively. On the right panel, MWA 185-MHz contours start at 2σ and proceed in $\sigma = 100$ mJy increments.

3.6 K, similar to the background temperature of the whole region. Given that we know the location of the expected emission from the radio lobes, we use the 2σ sensitivity of the image to estimate an upper limit on the flux density of the radio lobes at 1.4 GHz. The 1σ RMS is 18 mJy beam^{-1} and the radio lobes occupy two $14'.4$-FWHM Parkes beams, so an upper (2σ) flux density limit at 1.4 GHz is 72 mJy.

At 4.85 GHz, the Parkes-MIT-NRAO (PMN) survey (Condon, Griffith & Wright 1993) shows no detection of either a source at NGC 1534's position or of the diffuse radio lobes. Following a similar deduction as with CHIPASS, the 1σ RMS is 8 mJy beam^{-1} and the radio lobes occupy twelve 5 arcmin-FWHM Parkes beams, so an upper (2σ) flux density limit at 4.85 GHz is 200 mJy.

In summary, the MWA is the only instrument with the resolution and surface brightness sensitivity capable of making a reliable detection of the radio lobes, and their presence in the Molonglo data provides a useful flux density estimate at a higher frequency.

3.3   Radio structure and spectrum

NGC 1534 has extreme radio properties. In the MWA images the lobes are very diffuse with no sign of any jets or hot spots. Fitting a power law spectrum ($S \propto \nu^\alpha$) to the MWA and SUMSS measurements, and the CHIPASS upper limit (see Figure 5), we derive a spectral index $\alpha = -2.1 \pm 0.1$ for the lobes. This is much steeper than typical radio galaxies with active central jets. We note that the CHIPASS flux density could be lower, which would lead to a spectrum with a break.

No nuclear source is detected by the MWA and the peak brightness at NGC 1534's position is 270 mJy beam^{-1}. We look to ancillary data to place limits on the core flux density.

No source is visible in the Australia Telescope 20 GHz

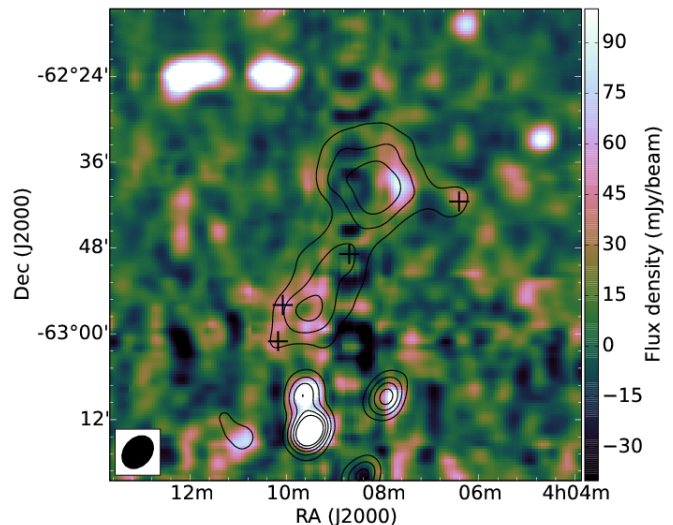**Figure 4.** 408 MHz image of the NGC 1534 region from MRCR. MWA 185-MHz contours start at 2σ and proceed in $\sigma = 100$ mJy increments; the MWA synthesised beam is shown as a filled ellipse in the lower-left corner. The MRCR beam is $3'.2 \times 2'.6$ (position angle 0°). Unfortunately, the N-S sidelobes of PKS 0408−65 bisect the lobes of NGC 1534 and leave a negative residue. The two bright "sources" to the NE are E-W sidelobes of PKS 0420−62. The MWA synthesised beam is shown as a filled ellipse in the lower-left corner.

survey (Murphy et al. 2010), and the RMS noise level at its position is 5.7 mJy beam^{-1} (Hancock 2014, priv. comm.), so we give a 2σ upper limit of 11 mJy. Similarly, given an RMS noise level of 7.8 mJy beam^{-1} in the 4.85 GHz PMN survey, a 2σ upper limit of 15.6 mJy beam^{-1} can be placed. The peak brightness in the unsmoothed SUMSS data

Table 4. Sources detected within the radio lobes as measured by the SUMSS radio survey. The two columns with "*"s show extrapolated flux densities at the MRCR and MWA observing frequencies using a spectral index α of -0.7. One source is not subtracted from the MRCR data, as it lies in the region of the poorly-subtracted grating lobe, so we do not list its predicted flux density.

RAJ2000	DEJ2000	$S_{843\mathrm{MHz}}$ (mJy)	$S^*_{408\mathrm{MHz}}$ (mJy)	$S^*_{185\mathrm{MHz}}$ (mJy)
04 06 27.54	$-62\ 41\ 44.50$	21.7 ± 1.1	36.1 ± 1.8	64.0 ± 3.2
04 08 41.52	$-62\ 49\ 09.20$	17.5 ± 1.1	–	51.6 ± 3.2
04 10 03.30	$-62\ 56\ 15.20$	12.4 ± 1.1	20.6 ± 1.8	36.5 ± 3.2
04 10 09.43	$-63\ 01\ 19.30$	27.8 ± 2.6	46.2 ± 4.3	81.9 ± 7.7
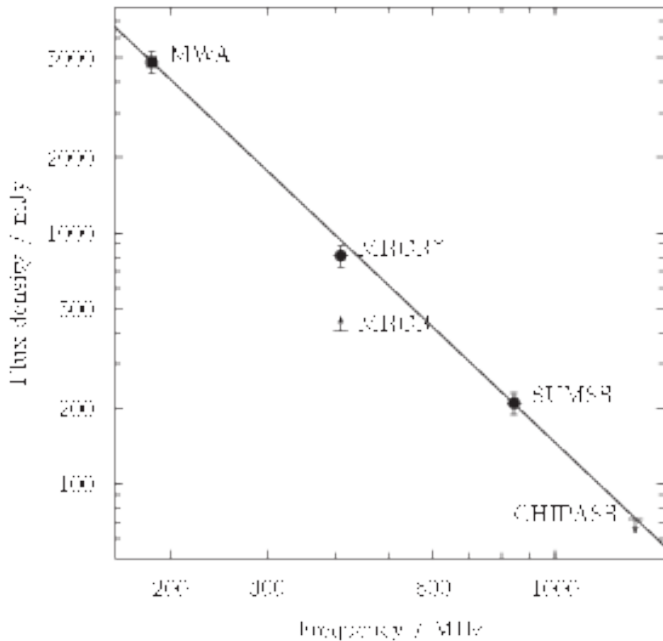
Figure 5. Plot of the measured values of the flux density of the radio lobes of NGC 1534 at 185, 408, 843 and 1400 MHz, from MWA, MRCR, SUMSS and CHIPASS, respectively, as shown in Table 2. The line indicates a least-squares unweighted fit made to the MWA and SUMSS measurements and CHIPASS upper limit, with a spectral index of $\alpha = -2.1 \pm 0.1$.

is $2.07\,\mathrm{mJy\,beam}^{-1}$. Initial exploratory observations made with the Australia Telescope Compact Array at 1.4 GHz result in a 2σ upper limit of $0.2\,\mathrm{mJy\,beam}^{-1}$. Further observations of the core will be presented in Johnston-Hollitt et al. (in prep).

Using the 1.4 GHz measurement as the strongest limit, and assuming a typical flat-spectrum core, we scale to 843 MHz in order to compare with the results of Saripalli et al. (2005). We find that the core is responsible for $< 0.1\%$ of the total flux density at 843 MHz. This is a factor of two fainter than the faintest cores compiled by Saripalli et al., implying very little emission from an active accretion disk.

4 DISCUSSION

4.1 Radio galaxies with disks

Highly extended radio sources hosted by galaxies with disks are very rare, with only six other clear examples known:

- **J 2345-0449**, recently discovered to be the largest radio galaxy associated with a spiral (Bagchi et al. 2014);
- **Speca** (SDSS J 140948.85-030232.5; Hota et al. 2011), which has an inner steep-spectrum double and an outer relic lobe, part of which is re-accelerated and flatter-spectrum;
- **PKS 0131-36** (NGC 612; Emonts et al. 2008), which posseses a huge disk of cool H I gas distributed along the optical disk and dust lane;
- **Fornax A** (NGC 1316; Ekers et al. 1983), whose dust lane is harder to see due to its face-on orientation;
- **Centaurus A** (NGC 5128; Bolton, Stanley & Slee 1949), which was recently imaged in detail by Feain et al. (2011);
- **0313-192** (PMN J0315-906) (6dFGS gJ031552.1-190644; Ledlow et al. 2001), a 200 kpc double-lobed radio galaxy with a disk.

In Table 5 we give the physical properties of these objects, and do not include the numerous examples of radio galaxies hosted by elliptical galaxies with small-scale circum-nuclear disks, or disk galaxies with smaller-scale emission such as B2 0722+30, a H I-rich spiral galaxy with $\approx 14\,\mathrm{kpc}$ radio jets aligned in a manner suggesting tidal interactions with other nearby galaxies (Emonts et al. 2009).

It has always been notable that the powerful double-lobed radio galaxies are identified with giant elliptical galaxies and are almost never found associated with spiral galaxies (Véron-Cetty & Véron 2010). However, those radio galaxy hosts with disks or dust lanes are particularly interesting since they make it possible to trace the dynamics of the gaseous material which is assumed to be the source of fuel in these systems. For instance, in the case of NGC 612, Emonts et al. (2008) discovered an enormous disk of cool gas with $M_{\mathrm{H I}} = 1.8 \times 10^9 M_\odot$ distributed along the optical disk and dust lane. NGC1534 has a prominent dust lane, and hence must have a gaseous disk, but it is not yet detected in H I, with a mass limit from the HIPASS survey of $< 1.0 \times 10^{10}\,\mathrm{M}_\odot$.

Using the infrared flux densities (Table 3) measured by Infrared Astronomical Satellite (IRAS), and the infrared luminosity-dust temperature relation (Equation 3) of Young et al. (1989) adapted to IRAS 60- and 100-μm flux densities in Equation 7 of Roberts et al. (1991), we derive a characteristic dust temperature of $24 \pm 2\,\mathrm{K}$. This is quite cool: generally $T_{\mathrm{dust}} > 30\,\mathrm{K}$ in galaxies with moderate on-going star formation. The estimated dust mass is $1.8 \times 10^7\,\mathrm{M}_\odot$, which is similar to that in other early-type galaxies with prominent dust lanes. Given the typical gas/dust ratio for early-type galaxies with dust lanes, we would expect to see of order $10^{10}\,\mathrm{M}_\odot$ of HI associated with this cool dust, which suggests that the current upper limit must be close to the

Table 5. Properties of known disk galaxies hosting large (linear size > 100 kpc) radio lobes. $L_{325\mathrm{MHz}}$ and α refer to the 325-MHz luminosity and spectral index of the radio lobes.

Name	z	Linear size (kpc)	Total $L_{325\mathrm{MHz}}$ (W Hz^{-1})	α	M_K
2MASX J 23453268-0449256	0.07860 (a)	1580 (b)	5.2×10^{25} (b)	−2.0 (b)	−26.0 (c)
NGC 612 (PKS 0131-36)	0.030 (d)	500 (e)	3.2×10^{25} (f)	−0.51 (f)	−25.9 (c)
SDSS J 140948.85-030232.5 (Speca)	0.14 (g)	1300 (h)	2.3×10^{25} (h)	−0.8 (h)	−25.6 (c)
NGC 1316 (Fornax A)	0.00591 (d)	389 (i)	2.2×10^{25} (i)	−0.77 (i)	−26.3 (c)
NGC 5128 (Centaurus A)	0.0018 (j)	500 (k)	5.5×10^{24} (k)	−0.64 (l)	−25.4 (c)
6dFGS gJ031552.1-190644 (0313-192)	0.067 (m)	200 (n)	2.5×10^{24} (n)	unknown	−24.7 (c)
NGC 1534	0.018 (d)	700 (o)	9.7×10^{23} (o)	−2.1 (o)	−25.0 (c)

References: (a) Mauch & Sadler (2007); (b) Bagchi et al. (2014); (c) Skrutskie et al. (2006); (d) Paturel et al. (2002); (e) Emonts et al. (2008); (f) Wall & Peacock (1985); (g) Adelman-McCarthy & et al. (2009) (h) Hota et al. (2011); (i) McKinley et al. (2014); (j) Lavaux & Hudson (2011); (k) Cooper, Price & Cole (1965); (l) McKinley et al. (2013); (m) Owen, Ledlow & Keel (1995); (n) Ledlow, Owen & Keel (1998); (o) This paper.

actual value, and this galaxy ought to be detectable in HI with only a modest amount of additional observing time. Furthermore, the HI morphology and kinematics might give some additional hints about the past history of this galaxy.

Schoenmakers et al. (2001) have compiled a sample of Giant Radio Galaxies from the Westerbork Northern Sky Survey (WENSS; Rengelink et al. 1997) and a survey of the literature. Rescaling our 185 MHz flux density to 325 MHz, assuming $\alpha = -2.1$, we calculate the NGC 1534 radio jet luminosity at 325 MHz as 9.7×10^{23} W Hz^{-1}. We replot Figure 3 of Schoenmakers et al. with our cosmology in Figure 6, and see that NGC 1534 is inaccessible to a survey with the sensitivity of WENSS; Schoenmakers et al. note that low-redshift objects of linear size less than 1 Mpc cannot be detected due to the low angular size limit of WENSS, while at higher redshifts they become faint and lie below the sensitivity threshold ($\approx 10^{25}$ W Hz^{-1} for $z = 0.1$). The lobes of NGC 1534 are considerably fainter and larger than the typical FR-I and II radio galaxies compiled by Laing, Riley & Longair (1983), which are powerful sources with active nuclei. We also include in the figure the eighteen GRGs discovered by Saripalli et al. (2005) using SUMSS, by scaling their 843 MHz luminosities to 325 MHz with a spectral index of −0.85.

The radio galaxies with disks (Table 5) are plotted in Figure 6 for comparison. They cover the same range of linear sizes but have somewhat lower radio luminosities, excepting the recently-discovered J 2345-0449. Their generally lower luminosities are probably a selection effect because the dust lanes and disks in early type galaxies may not be so easily identified in the more distant and more powerful sources.

The giant radio galaxy J 0034.0-6639, observed in the Australia Telescope Low Brightness Survey (ATLBS; Saripalli et al. 2012) had the lowest surface brightness lobes known: 1 mJy arcmin^{-2} at 1.4 GHz. J 0034.0-6639 is 17 arcmin in extent, which is half the angular size of NGC 1534, but at a redshift of 0.11 it is six times more distant and hence three times our linear size at 2 Mpc. It has quite similar radio morphology to NGC 1534 and is aligned with the minor axis of an E galaxy. Scaled to 1.4 GHz assuming $\alpha = -2.1$, we calculate that the radio lobes of NGC 1534 have a surface brightness of less than 0.1 mJy arcmin^{-2}, making it the lowest-surface-brightness giant radio galaxy detected, by an order of magnitude.
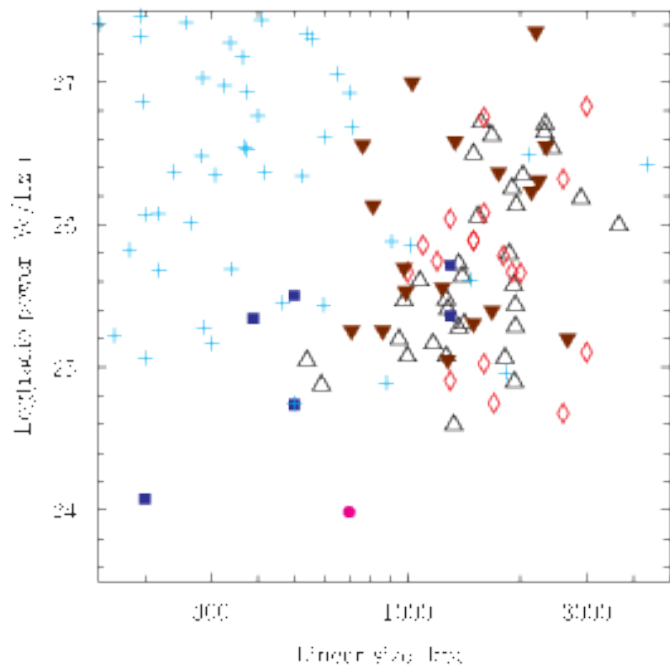

Figure 6. The 325-MHz radio power against linear size $P - D$ diagram for GRGs in the literature: FR-I and FR-II objects compiled by Laing, Riley & Longair (1983) with $z < 0.6$, scaled by a spectral index of −0.8 following Schoenmakers et al. (2001) (plusses), GRGs discovered before 1998 (diamonds), GRGs discovered by Schoenmakers et al. (2001) (empty triangles), GRGs measured by Saripalli et al. (2005) (filled triangles), the radio lobes of NGC 1534 as described in this paper (filled circle) and the six other radio galaxies hosted by galaxies with disks whose properties are given in Table 5 (filled squares).

4.2 A relic giant radio galaxy?

The lobes hosted by NGC 1534 are certainly in the regime which makes them dim enough to be a true relic, but are physically smaller than the lobes of the GRGs compiled by Schoenmakers et al. (2001). As 'relic' radio galaxies age, if the electrons are not re-accelerated, the jets become large and dimmer, and the spectral index steepens. The spectral index of the lobes of NGC 1534, $\alpha = -2.1$, is comparable to the steepest spectra seen in other dying radio sources (e.g. Murgia et al. 2011). The lack of a central source implies that

AGN activity has halted, sufficiently long ago for the lobes to age. Is there too little gas available as fuel, or is none being transported into the central black hole?

Murgia et al. (2011) have shown that relic sources selected by their steep spectra are much more likely to be found in dense environments. This is important because when an AGN ceases to be active, it is expected that the lobes will expand and cool, but this is only the case in underdense environments. For such sources found in environments of medium to high density, such as galaxy clusters, the intracluster medium is expected to prevent much expansion, effectively maintaining the lobe. Thus, in the early stages after AGN activity ceases, the observational properties of the lobes of 'dead' radio galaxies in dense environments may vary little from those that are still active, whereas in underdense regimes the lobes may freely expand giving rise to significantly dimmer objects with very steep spectral indices over similar timescales. Precise comparisons, however, require detailed knowledge of the environment (including the properties of ambient and lobe magnetic fields) and an understanding of the age of the emission. Although NGC 1534 is associated with a widely dispersed galaxy group, it is unlikely to lie within a medium capable of preventing the lobe expansion; this is, again, consistent with it being a true 'relic' galaxy.

4.3 Other possible origins?

The physical size and proximity of the radio source to the nearest catalogued galaxy cluster, A 3229 (Abell, Corwin & Olowin 1989) suggest that the emission might not be a GRG, but rather a radio relic on the outskirts of the cluster. However, investigations into A 3229 suggest that it is not, in fact, a galaxy cluster. Abell, Corwin & Olowin (1989) do not assign a redshift in the original identification; Mould et al. (1991) assign it a redshift of 0.017 based on a cross-match with the object DC 0410-62 identified by Dressler (1980), while it is reported in the NASA Extragalactic Database as having redshift 0.091923, based on a cross-match with the initial 6dF data release (Jones et al. 2004). Examining the redshifts of the nearby galaxies as given by the final version of the 6dF galaxy survey (Jones et al. 2009) shows that there is no local overdensity of galaxies at $z \approx 0.09$, and that the nearest true galaxy cluster is A 3266, part of the Horologium-Reticulum Supercluster (HRS) (Fleenor et al. 2005). The HRS is one of the most massive galaxy concentrations in the local Universe and is expected to host many dynamical events which might generate radio relics. However, for the observed lobes to be relic emission associated with the nearest cluster, they would need to lie 12 Mpc away, which puts the emission beyond the limit of where simulations predict large-scale structure formation shocks can occur (Miniati et al. 2001).

As previously noted, Crook et al. (2007) identify NGC 1534 as belonging to the galaxy group HDC 269 at $z = 0.017$. There is no sign of X-ray emission in the RÖntgenSATellit (Trümper 1984, ROSAT) All-Sky Survey data at its position, which, given the nearby redshift of the HRS, confirms this as a group, rather than a cluster. We conclude that A 3229 itself was misidentified as a cluster due to the chance alignment of HDC 269 and the outskirts of the Horologium-Reticulum Supercluster, and that the lobes seen around NGC 1534 cannot be relic emission from a cluster of galaxies.

Alternatively, the emission could be associated with a more distant radio galaxy. The general alignment between the radio lobes and NGC 1534 is quite reasonable (the position angles are nearly perpendicular, differing by 84°), although there are no inner jets or nuclear source to confirm the identification. Assuming the cosmology given in Section 1, the linear extent of the radio lobes is ≈ 700 kpc. If the identification with NGC 1534 is incorrect it must be associated with a more distant galaxy and the linear size would be much more extreme, and its radio power would be correspondingly larger.

4.4 The population of low surface brightness radio galaxies

At the time of the discovery of the lobes surrounding NGC 1534, around 4,000 deg^2 of sky had been imaged by the MWA with similar sensitivity to the observations described here, and examined to the same level of attention. This does not include the commissioning observations performed by Hurley-Walker et al. (2014) as they lacked the surface brightness-sensitivity of the full array. In this entire sky area, only one such object has been detected, although a concerted search of the full sky area accessible to the MWA has not yet begun. We note that the GaLactic and Extragalactic All-sky MWA survey (GLEAM; Wayth et al. in prep) will integrate for a similar amount of time for the whole sky south of Declination $+30°$ over a wider frequency range of 75–230 MHz, allowing the calculation of the spectral index of such objects from MWA data alone, which will give a more uniform sampling of spatial scales than the range of instruments used in this paper.

GRGs have very low brightness and will be fully resolved in any high resolution survey so it is possible that there is an undiscovered population of such sources; see e.g. Saripalli et al. (2012). Assuming that GRGs are randomly distributed over the southern sky, and that GLEAM reaches the same sensitivity as the observations in this paper, we can only expect a few (< 10) more objects of this brightness, so it will remain a rare population. Serendipitously, NGC 1534 did not coincide with any bright (unrelated) sources at MWA frequencies; to best search for diffuse objects such as relic radio lobes, contaminating unrelated sources will need to be peeled. Assuming this can be done, diffuse sources with peak surface brightness of ≈ 80 mJy beam^{-1} should be reliably detectable, which could unveil an even fainter population of relic sources.

4.5 Relative lifetime and space density

Luo & Sadler (2010) present analytic models for the time evolution of low-power radio galaxies at 1.4 GHz, applied to a subset of local ($z = 0.02$–0.3) Two-degree-Field Galaxy Redshift Survey (2dFGRS; Colless 1999) radio galaxies. We note that NGC 1534 would not appear in this sample as it has a surface brightness below the 2dFGRS sample radio detection limit (see Figure 3 of Luo & Sadler 2010).

In Figure 7, we reproduce Figure 8 of Luo & Sadler (2010), which shows the evolution of high-luminosity (FR-II)
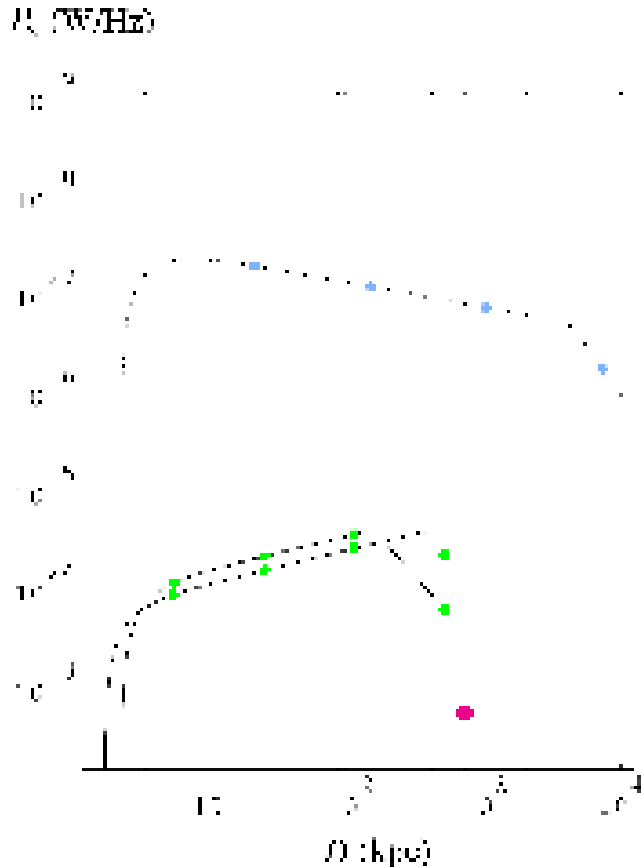
Figure 7. A reproduction of Figure 8 of Luo & Sadler (2010), showing the evolutionary (1.4 GHz-)power-size tracks for high-luminosity (FR-II) sources (dashed) and low-luminosity (FR-I) sources (solid). The dots (from left to right) on each curve indicate ages; for low-luminosity sources, of interest here, the green (lower) dots represent $1\,\mathrm{Myr}$, $10\,\mathrm{Myr}$, $10^2\,\mathrm{Myr}$, and $10^3\,\mathrm{Myr}$, for two slightly different models of radio galaxy evolution (see Luo & Sadler 2010, for more details). The (scaled 1.4-GHz) power and size of NGC 1534 is overlaid with a large magenta circle.

and low-luminosity (FR-I) sources in power and linear size according to the described models. The power-size tracks are characterized by a slow increase in both size and luminosity over most of the source lifetime, followed by a rapid decline in luminosity at late times. Assuming that the extent of the lobes of NGC 1534 is the same at 1.4 GHz as observed in the MWA data, and that the CHIPASS upper limit is its true luminosity, we can overlay NGC 1534 in the same plot. We see that it lies in the region of the *P-D* diagram which corresponds to a low-power radio galaxy at the end of its life, with an age $> 10^9\,\mathrm{yr}$. In this model the peak radio luminosity of the lobes of NGC 1534 would have been at most a few times $10^{24}\,\mathrm{W\,Hz^{-1}}$, and perhaps a little lower. Note that the 1.4-GHz extent could be smaller, and the spectrum may curve downward at higher frequencies, so its position in Figure 7 is likely to be an upper limit.

Since NGC 1534 may have been caught in the rare dying phase, it is of interest to estimate the space density for such objects and hence the fraction of time an AGN might spend in this phase. NGC 1534 is the only double-lobed source of this angular size in the $4{,}000\,\mathrm{deg}^2$ area surveyed so far. Sim-

ilar sources could have been detected at up to twice this distance, corresponding to a volume of $1.5 \times 10^6\,\mathrm{Mpc^3}$. Thus the space density is $\approx 7 \times 10^{-7}\,\mathrm{Mpc^{-3}}$; our result is roughly seven times greater than that of Saripalli et al. (2005) due to the higher surface brightness sensitivity of the MWA compared to SUMSS.

Using the bivariate luminosity function from Mauch & Sadler (2007), we estimate that there are 15 AGN in this volume with radio luminosities greater than or equal to that of NGC 1534 and identified with similar brightness elliptical galaxies. Hence we can argue that normal AGN cannot spend more than 6% of their lifetime in this phase if they all go through the same cycle. Of course it is possible that some AGN may not reach this linear size (e.g. those more confined in galaxy clusters) and may have a longer lifetime in the dying phase. To refine this estimate we would need to compare objects of similar linear size separating those with no evidence for ongoing energy input based on the absence of cores and hot spots and with a cut-off in their spectra. The spectral search will be possible with the GLEAM survey, now in progress. Determining the presence of cores and hotspots will require higher resolution surveys such as those to be carried out by the Australian SKA Pathfinder, and eventually SKA-mid.

5   CONCLUSION

We report the discovery of the lowest surface brightness radio galaxy yet detected, associated with the lenticular galaxy NCG 1534. This represents only the seventh detection of large-scale radio lobes associated with a galaxy containing a dust lane. Additionally, NCG 1534 has the steepest spectral index and lowest power of galaxies of this type. The lack of jets, hotspots and an obvious radio core associated with the optical host along with the non-detection of significant neutral hydrogen, despite the obvious dust lane, suggest that this is a true "relic" radio galaxy.

Deep observations at higher frequencies would be valuable in constraining the precise nature of the spectrum and in particular determine likely emission timescales and scenarios. Additionally, deep, high-resolution observations are required to better determine the core to lobe luminosity, as it is needed to confirm that the AGN is truly "dead". A measurement of the H I mass would help determine whether there is any material available to feed the central black hole.

In the next few years LOFAR and the MWA will conduct a series of all-sky continuum radio surveys and will undertake a wide range of survey science projects (Norris et al. 2013). These surveys have the potential to uncover more systems of this type, although the expected source density remains low. With the advent of the SKA a decade hence, we will see a dramatic improvement in sensitivity to the population of "relic" radio galaxies and may perhaps detect them in sufficient numbers to start to undertake detailed statistical analysis of the population as a whole.

REFERENCES

Abell G. O., Corwin, Jr. H. G., Olowin R. P., 1989, ApJS, 70, 1

Adelman-McCarthy J. K., et al., 2009, VizieR Online Data Catalog, 2294, 0

Bagchi J. et al., 2014, ApJ, 788, 174

Barnes D. G. et al., 2001, MNRAS, 322, 486

Bock D. C.-J., Large M. I., Sadler E. M., 1999, AJ, 117, 1578

Bolton J. G., Stanley G. J., Slee O. B., 1949, Nature, 164, 101

Briggs D. S., 1995, in Bulletin of the American Astronomical Society, Vol. 27, American Astronomical Society Meeting Abstracts, p. 112.02

Broderick J. W., Bryant J. J., Hunstead R. W., Sadler E. M., Murphy T., 2007, MNRAS, 381, 341

Calabretta M. R., Staveley-Smith L., Barnes D. G., 2014, PASA, 31, 7

Colless M., 1999, Royal Society of London Philosophical Transactions Series A, 357, 105

Condon J. J., Griffith M. R., Wright A. E., 1993, AJ, 106, 1095

Cooper B. F. C., Price R. M., Cole D. J., 1965, Australian Journal of Physics, 18, 589

Crook A. C., Huchra J. P., Martimbeau N., Masters K. L., Jarrett T., Macri L. M., 2007, ApJ, 655, 790

de Vaucouleurs G., de Vaucouleurs A., Corwin, Jr. H. G., Buta R. J., Paturel G., Fouqué P., 1991, Third Reference Catalogue of Bright Galaxies. Volume I: Explanations and references. Volume II: Data for galaxies between 0^h and 12^h. Volume III: Data for galaxies between 12^h and 24^h.

Dressler A., 1980, ApJS, 42, 565

Ekers R. D., Goss W. M., Wellington K. J., Bosma A., Smith R. M., Schweizer F., 1983, A&A, 127, 361

Emonts B. H. C., Morganti R., Oosterloo T. A., Holt J., Tadhunter C. N., van der Hulst J. M., Ojha R., Sadler E. M., 2008, MNRAS, 387, 197

Emonts B. H. C., Tadhunter C. N., Morganti R., Oosterloo T. A., Holt J., Brogt E., van Moorsel G., 2009, MNRAS, 396, 1522

Feain I. J. et al., 2011, ApJ, 740, 17

Fleenor M. C., Rose J. A., Christiansen W. A., Hunstead R. W., Johnston-Hollitt M., Drinkwater M. J., Saunders W., 2005, AJ, 130, 957

Green D. A., 2011, Bulletin of the Astronomical Society of India, 39, 289

Hindson L. et al., 2014, MNRAS, 445, 330

Hota A. et al., 2011, MNRAS, 417, L36

Hurley-Walker N. et al., 2014, ArXiv e-prints

Jones D. H. et al., 2009, MNRAS, 399, 683

Jones D. H. et al., 2004, MNRAS, 355, 747

Laing R. A., Riley J. M., Longair M. S., 1983, MNRAS, 204, 151

Large M. I., Mills B. Y., Little A. G., Crawford D. F., Sutton J. M., 1981, MNRAS, 194, 693

Lavaux G., Hudson M. J., 2011, MNRAS, 416, 2840

Ledlow M. J., Owen F. N., Keel W. C., 1998, ApJ, 495, 227

Ledlow M. J., Owen F. N., Yun M. S., Hill J. M., 2001, ApJ, 552, 120

Lonsdale C. J. et al., 2009, IEEE Proceedings, 97, 1497

Luo Q., Sadler E. M., 2010, ApJ, 713, 398

Mauch T., Murphy T., Buttery H. J., Curran J., Hunstead R. W., Piestrzynski B., Robertson J. G., Sadler E. M., 2003, MNRAS, 342, 1117

Mauch T., Sadler E. M., 2007, MNRAS, 375, 931

McKinley B. et al., 2013, MNRAS, 436, 1286

McKinley B. et al., 2014, ArXiv e-prints

Miniati F., Jones T. W., Kang H., Ryu D., 2001, ApJ, 562, 233

Mould J. R. et al., 1991, ApJ, 383, 467

Murgia M. et al., 2011, A&A, 526, A148

Murphy T. et al., 2010, MNRAS, 402, 2403

Neugebauer G. et al., 1984, ApJL, 278, L1

Norris R. P. et al., 2013, PASA, 30, 20

Owen F. N., Ledlow M. J., Keel W. C., 1995, AJ, 109, 14

Paturel G., Dubois P., Petit C., Woelfel F., 2002, LEDA, 0 (2002), 0

Rengelink R. B., Tang Y., de Bruyn A. G., Miley G. K., Bremer M. N., Roettgering H. J. A., Bremer M. A. R., 1997, A&AS, 124, 259

Roberts M. S., Hogg D. E., Bregman J. N., Forman W. R., Jones C., 1991, ApJS, 75, 751

Saripalli L., Hunstead R. W., Subrahmanyan R., Boyce E., 2005, AJ, 130, 896

Saripalli L., Subrahmanyan R., 2009, ApJ, 695, 156

Saripalli L., Subrahmanyan R., Thorat K., Ekers R. D., Hunstead R. W., Johnston H. M., Sadler E. M., 2012, ApJS, 199, 27

Schoenmakers A. P., de Bruyn A. G., Röttgering H. J. A., van der Laan H., 2001, A&A, 374, 861

Skrutskie M. F. et al., 2006, AJ, 131, 1163

Tingay S. J. et al., 2013, PASA, 30, 7

Trümper J., 1984, Physica Scripta Volume T, 7, 209

van Haarlem M. P. et al., 2013, A&A, 556, A2

Véron-Cetty M.-P., Véron P., 2010, A&A, 518, A10

Wall J. V., Peacock J. A., 1985, MNRAS, 216, 173

Wright A., Otrupcek R., 1990, in PKS Catalog (1990), p. 0

Young J. S., Xie S., Kenney J. D. P., Rice W. L., 1989, ApJS, 70, 699